Desalination and Water Treatment
www.deswater.com

doi: 10.5004/dwt.2020.25291

188 (2020) 390–399
June

The leakage analysis of submarine pipeline connecter based on a new fractal porous media model

Ming Liu[a], Lan Zhang[a,*], Liquan Wang[a], Hengxu Liu[b], Yongquan Sun[a], Yingjun Wang[a]

[a]*College of Mechanical and Electrical Engineering, Harbin Engineering University, Harbin 150001, China*
[b]*College of Shipbuilding Engineering, Harbin Engineering University, Harbin 150001, China, email: zhanglan@hrbeu.edu.cn (L. Zhang)*

Received 16 July 2019; Accepted 18 December 2019

ABSTRACT

The leakage mechanism of the clamp connector for submarine pipeline is investigated. The contact seal of a clamp connector is regarded as a half-cylinder squeezing a plane. Moreover, mean stress of the contact region is used to calculate the permeability, based on an observation length-dependent mechanic model and a new fractal porous media model. The analysis yields insight into the effects of surface fractal parameters on the permeability, when mean stress rises within the yield limit. Compared with experiment results, the prediction of this model shows well consistency in the trend.

Keywords: Submarine pipeline connecter; Contact seal; Observation length-dependent mechanics model; Fractal porous media model; Leakage analysis

1. Introduction

Offshore oil and gas development has gradually become an important part of global energy growth, as land resources dried up. Submarine pipeline connectors are widely used in underwater oil extraction system. The seal of two contact surfaces plays an important role in typical connectors, such as clamp connector, bolted flange connector, collet connector, and pipeline stopper. The failure of seals results in catastrophic consequences, such as oil spills, the Marine environment pollution, and marine life extinction. Since machined surfaces usually have roughness and fractal character, micropores, and leakage channels can be observed in the contact seal region, even in ultra-tight seal.

The contact seal have attracted research interest of scholars. Ji et al. [1] reviewed the recent research of contact seal and discussed a leakage model based on percolation theory. Feng and Gu [2] and Feng [3] suggested a leakage model for metal flat gasket, based on MB fractal contact model and the laminar flow theory of incompressible viscous fluid. He studied the effects of fractal parameters on leakage characteristics and conducted experiments to prove his theory. Shi [4] proposed a leakage model of contact static seal based on the percolation model, and studied the effect of element shape on the percolation threshold and leakage characteristics. Persson [5] and Persson and Yang [6] presented a theory of the leak-rate of seals, which was based on percolation theory and a contact mechanics theory. Lorenz and Persson [7] presented experimental results for the leak rate of rubber seals and compared the results to Persson's theory. The results showed good agreement between theory and experiment. When the contact between two surfaces is quite sufficient, the application of a porous medium model is more reasonable to describe the fluid flow between the seal region [8]. Yu [9] and Yu and Li [10] derived a unified model to describe the fractal characteristics of porous media, and proposed a criterion for judging whether the porous medium has fractal characteristics. Huang et al. [11] proposed a leakage model based on MB model and fractal porous medium model. The gas leakage of metal gasket was predicted, which was consistent with the experiment. Liu et al. [12] studied the effects of fluid pressure change on leakage of contact seal based on a fractal porous media model.

However, there is still a lack of research on the contact seal of the surface with macroscopic non-flat geometry. In this work, the leakage mechanism of clamp connector was investigated based on contact mechanic model and leakage model. An observation length-dependent (OLD) mechanic model was applied to analyze contact mechanism

* Corresponding author.

of isotropic fractal rough surfaces. Therefore, a fractal porous media model was proposed to calculate the permeability of contact surface, based on the critical observation length. A leakage experiment of clamp connector was carried out to verify the theory.

2. Mechanics and leakage models of clamp connector

2.1. Contact seal of clamp connector

The subsea clamp connector adopts a typical contact seal of a sphere and a cone, which consists of a metal lens seal ring and flanges, respectively, as shown in Fig. 1. The contact seal can be regarded as a half cylinder squeezing a plane. Moreover, the seal region is a rectangle with length L and width $2r$. Oil and gas leak from one side of the seal region to the other along the width, as shown in Fig. 2.

The half of the contact width r can be calculated by Hertz theory [13],

$$r = \sqrt{\frac{4F_L R}{\pi E^* L}} \tag{1}$$

where F_L is the normal load, R is the radius of the cylinder, E^* is the equivalent modulus of Hertzian elasticity, $1/E^* = (1 - v_1^2)/E_1 + (1 - v_2^2)/E_2$, E_1, E_2, v_1, and v_2 are Young's modulus and Poisson's ratios of two contacting surfaces, respectively.

The mean stress is:

$$\sigma_m = \frac{F_L}{2rL} \tag{2}$$

Since the width of seal region is very small, the contact of seal region can be simplified the contact of a rigid plane and a deformable fractal surface, as shown in Fig. 3. In addition, the mean stress is usually an important calculation parameter for the contact seal of submarine pipeline connection system [14–16].

2.2. Contact mechanics model

2.2.1. Ideal subplane

We have presented an OLD mechanic model to calculate the real contact area, recently. The profile height of surface $z(x)$ is defined by WM function [7,17]

$$z(x) = G^{D-1} \sum_{n=n_L}^{\infty} \frac{\cos\left(2\pi\gamma^n x\right)}{\gamma^{(2-D)n}} \tag{3}$$

where G is the fractal roughness parameter, D is the surface fractal dimension and $1 < D < 2$, γ^n determines the frequency spectrum of the surface roughness and for most typical surfaces, $\gamma = 1.5$. $n_L = \log_\gamma(1/L_0)$ and L_0 is the sample length.

The sample surface with length L_0 is assumed to be composed of ideal subplanes with length of λ, which is observation length and $0 < \lambda < L_0$, as shown in Fig. 4. A reference plane is defined, based on which the average height of the surface profile is zero, that is, $\langle z(x)\rangle = 0$, where $\langle\ldots\rangle$ is ensemble average.

The height of the ideal subplane is:

$$h(x,\lambda) = \left\langle z(x_i)\right\rangle \tag{4}$$

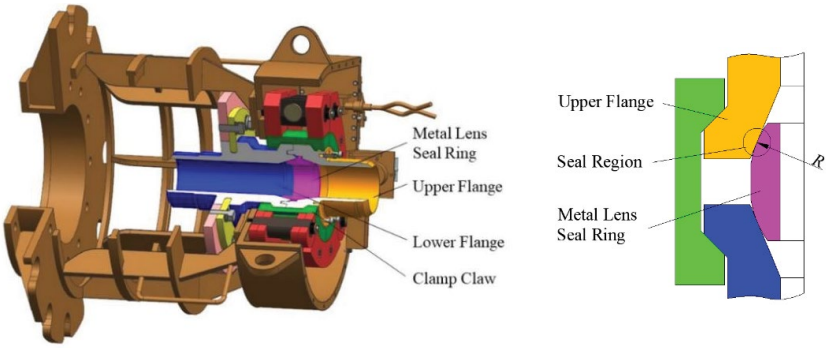

Fig. 1. Subsea clamp connector and contact seal.

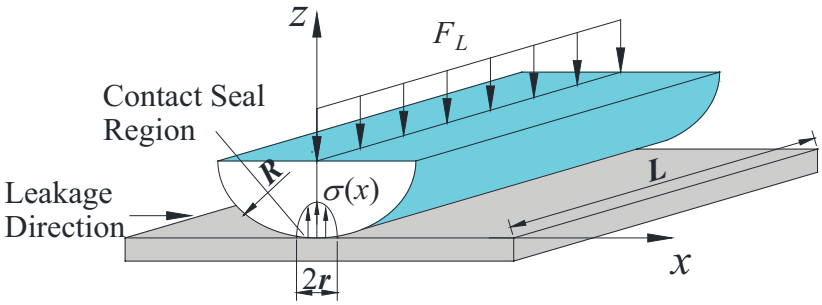

Fig. 2. The equivalent seal model of submarine pipeline connectors.

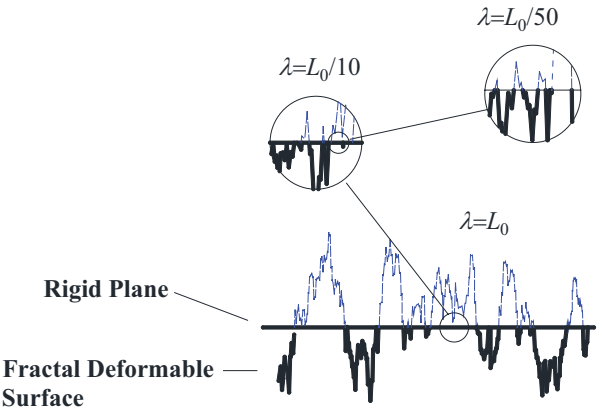

Fig. 3. A rigid plane contact with a fractal deformable surface.

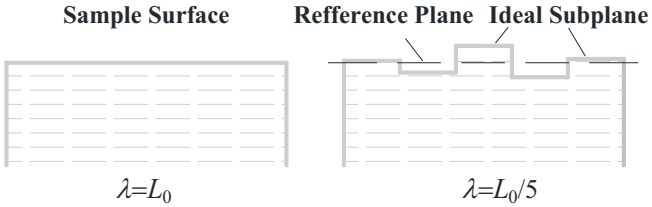

Fig. 4. Sketch of sample surface at $\lambda = L_0$ and ideal subplane at $\lambda = L_0/5$.

where x_i is the coordinate of the ideal subplane, in the range of $(-\lambda/2, \lambda/2)$.

According to the law of large numbers, it is assumed that the height of the ideal subplane obeys the Gaussian distribution. Therefore, the rough surfaces observed in different observation lengths conform to the Gaussian distribution, as shown in Fig. 5. The probability density of ideal subplane at observation length λ is:

$$\Phi'(h,\lambda)=\frac{1}{\sqrt{2\pi}\tau_h(\lambda)}\exp\left[-\frac{\left[h(x,\lambda)-\bar{h}(\lambda)\right]^2}{2\tau_h^2(\lambda)}\right] \tag{5}$$

where $\bar{h}(\lambda)$ is the mean height of the ideal subplane, $\bar{h}(\lambda)=\langle z(x,y)\rangle=0$. $\tau_h(\lambda)$ is the standard deviation of the ideal subplane height.

$$\tau_h(\lambda)=\left\{\left\langle\left[h(\lambda)-\bar{h}(\lambda)\right]^2\right\rangle\right\}^{1/2} \tag{6}$$

So that, Eq. (5) can be rewritten as

$$\Phi'(h,\lambda)=\frac{1}{\sqrt{2\pi}\tau_h(\lambda)}\exp\left[-\frac{h^2(\lambda)}{2\tau_h^2(\lambda)}\right] \tag{7}$$

Suppose a linear relationship applies, $\tau_h(\lambda)$ can be expressed as:

$$\tau_h(\lambda)=k_\tau\lambda+\tau_h(\delta),\left(\delta\le\lambda<L_0\right) \tag{8}$$

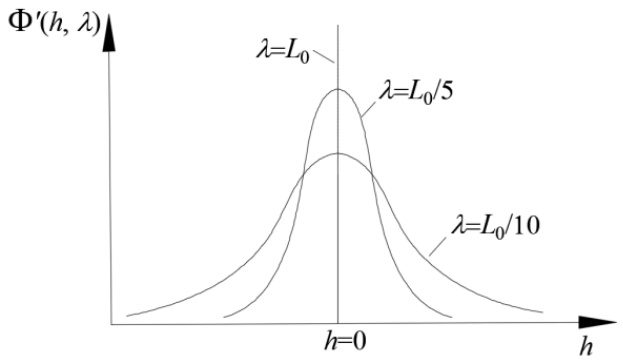

Fig. 5. Probability densities of the ideal subplane height, $\lambda = L_0$, $L_0/5$, and $L_0/10$.

where k_τ is the fitting slope, δ is the minimum observation length. $\tau_h(\delta)$ is the standard deviation of surface profile at δ, and could be calculated with fractal surface parameters [17,18]

$$\tau_h(\delta)=\frac{G^{D-1}}{\left[2(4-2D)\ln\gamma\right]^{1/2}}\left[L_0^{4-2D}-(2\delta)^{4-2D}\right]^{1/2} \tag{9}$$

2.2.2. Contact model of an ideal subplane

The contact of a rigid plane and a deformable rough surface can be idealized as the contact of a rigid plane and deformable ideal subplanes with a given observation length λ. It is assumed that the ideal subplanes are asperities of the same curvature radius.

According to MB model, the initial profile of asperity before deformation is:

$$h_p(x,\lambda)=G^{D-1}\lambda^{(2-D)}\cos\left(\frac{\pi x}{\lambda}\right),\left(-\frac{\lambda}{2}\le x\le\frac{\lambda}{2}\right) \tag{10}$$

The curvature radius of the asperity profile is:

$$R(\lambda)=\left|\frac{\left[1+\left(dh_p/dx\right)^2\right]^{3/2}}{d^2h_p(x,\lambda)/dx^2}\right|_{x=0}=\frac{\lambda^D}{G^{D-1}\pi^2} \tag{11}$$

The elastic contact force can be calculated with Hertz theory [5,13] as:

$$f_{el}(s)=\frac{4}{3}E^*R^{1/2}s_{el}^{3/2} \tag{12}$$

where s_{el} is the normal deformation of the asperity in elastic contact, as shown in Fig. 6.

The contact area of the asperity is:

$$a_{asp,el}=\pi R s_{el} \tag{13}$$

The contact area of the ideal subplane is:

$$a_{sub,el}=\lambda^2 \tag{14}$$

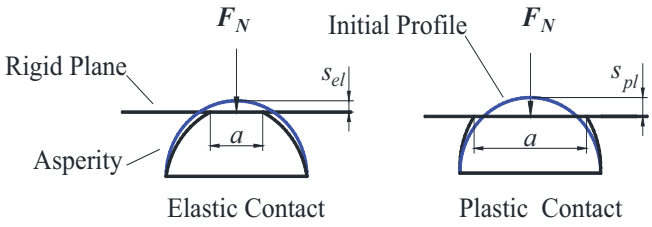

Fig. 6. Contact of asperity.

The sum of the contact area of subplanes is the real contact area of the contact surfaces. The contact area of the asperity is used to calculate the contact depth that will be used in subsection 2.3.

The critical deformation, s_c, of the plastic contact of a single asperity, is presented by Jackson and Green [19] based on Von Mises' yield criterion, as shown below:

$$s_c = \left(\frac{\pi C_Y \sigma_Y}{2E^*}\right)^2 R = \left(\frac{\pi C_Y \phi}{2}\right)^2 R \tag{15}$$

where C_Y is the yield strength coefficient obtained by curve fitting, C_Y = 1.295exp(0.736v). v is Poisson's ratio of the softer surface in the contact pairs. ϕ is the material property, $\phi = \sigma_Y/E^*$.

The plastic contact area of the asperity can be calculated by CEB model based on volume conservation [20].

$$a_{\text{asp,pl}} = \pi R s_{\text{pl}}\left(2 - \frac{s_c}{s_{\text{pl}}}\right) \tag{16}$$

where s_{pl} is the normal deformation of the asperity in plastic contact, $s_{\text{pl}} > s_c$.

The contact load of such an asperity is:

$$f_{\text{pl}} = \pi R s_{\text{pl}}\left(2 - \frac{s_c}{s_{\text{pl}}}\right) C_Y \sigma_Y \tag{17}$$

2.2.3. Contact areas and mechanics

According to WM model, the dimensionless real contact area of the sample surface is:

$$A_r^*(\lambda) = \int_{d(\lambda)}^{\infty} \Phi'(h,\lambda)\,dh \tag{18}$$

where $d(\lambda)$ is the distance between the rigid plane and the reference plane of the deformable fractal surface with the observation length, λ, as shown in Fig. 7.

The surface contact force consists of elastic and plastic parts:

$$F_N(\lambda) = F_{\text{el}}(\lambda) + F_{\text{pl}}(\lambda) \tag{19}$$

where $F_{\text{el}}(\lambda)$ and $F_{\text{pl}}(\lambda)$ are the elastic and plastic forces with the observation length of λ respectively, which can be calculated as the sum of elastic or plastic contact forces of asperities.

$$F_{\text{el}}(\lambda) = \frac{4E^*}{3\pi\lambda^2} A_0 R(\lambda)^{1/2} \int_{d(\lambda)}^{d_Y(\lambda)} \Phi'(h,\lambda)^{3/2}\,dh \tag{20}$$

$$F_{\text{pl}}(\lambda) = \pi C_Y \sigma_Y \frac{1}{\lambda^2} A_0 R(\lambda) \int_{d_Y(\lambda)}^{\infty} \Phi'(h,\lambda) s(h,\lambda)\left[2 - \frac{s_c(\lambda)}{s(h,\lambda)}\right] dh \tag{21}$$

where $s(h, \lambda)$ is the contact depth of the ideal subplane asperity, $s(h, \lambda) = h(x, \lambda) - d(\lambda)$. $d_Y(\lambda)$ is the plastic separation of the rigid plane and the reference plane of the deformable fractal surface at the observation length λ, $d_Y(\lambda) = d(\lambda) + s_c(\lambda)$.

Normalize contact force, F_N, with E^*A_0 as,

$$F_N^*(\lambda) = \frac{F_N(\lambda)}{E^* A_0} \tag{22}$$

Neglecting the effect of small probability events, the limits of the integral are $\pm k\tau_h(\lambda)$ and k = 3.

2.3. Fractal porous medium model

In this work, the seal region formed by contact surfaces can be regarded as the fractal porous medium composed of capillary bundles. Capillaries are tortuous touristy in the length direction, and any two couldn't intersect in the space, as shown in Fig. 8.

According to the investigations of Yu and his partners [10,21,22], the cumulative number of pore diameters in a unit cross-section of porous media has a fractal characteristic, and can be obtained by the fractal scaling law:

$$N(l \ge \ell) = \left(\frac{\ell_{\max}}{\ell}\right)^{D_p} \tag{23}$$

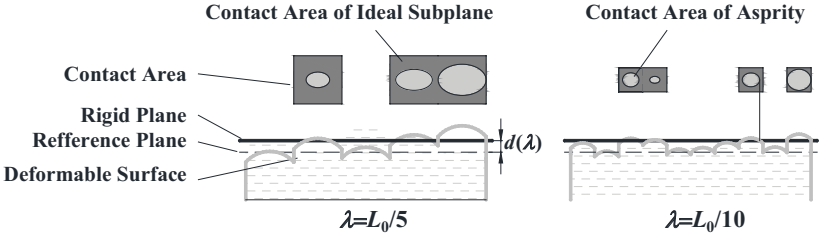

Fig. 7. Asperities of ideal subplane contact with a soft ideal plane.

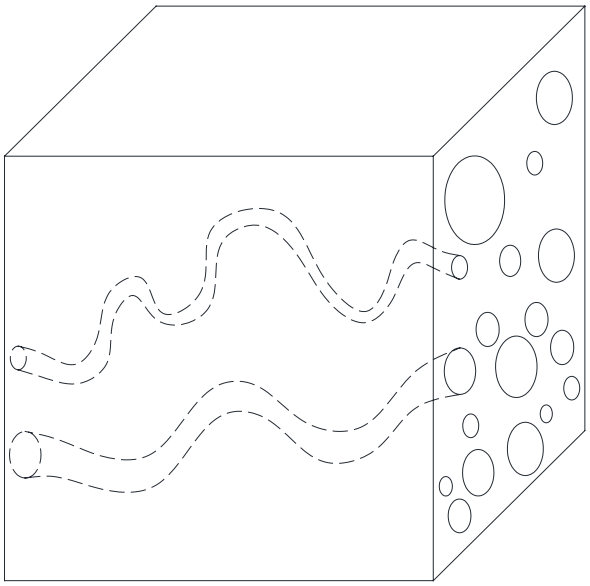

Fig. 8. A fractal porous medium model of a capillary bundle.

where N is the number of pores or capillaries, λ is the length scale, ℓ and ℓ_{max} are respectively the pore diameter and the maximum pore diameter. The fractal dimension D_p for pore spaces is in the range of $0 < D_p < 2$ in two dimensions.

Since the number of pores of porous media is very large, Eq. (23) in general is approximated as a continuous and differentiable function. The pores number in an infinitesimal range from ℓ to $\ell + d\ell$ can be obtained by differentiating Eq. (23) with respect to ℓ, that is,

$$-dN = D_p \ell_{\max}^{D_p} \ell^{-\left(D_p+1\right)} d\ell \tag{24}$$

where $-dN > 0$, the negative sign means that the pore number decreases with the increase of pore diameters. The pores in a unit cell (a set of fractal pores) can be considered as circles with different diameters ℓ. Therefore, the total pore area A_p in the cross-section of a unit cell (a set of fractal pores) can be calculated by the following formula, that is:

$$A_p = -\int_{\ell_{\min}}^{\ell_{\max}} \frac{1}{4}\pi\ell^2 dN = \frac{\pi D_p \ell_{\max}^2}{4\left(2-D_p\right)}\left[1-\left(\frac{\ell_{\min}}{\ell_{\max}}\right)^{2-D_p}\right] \tag{25}$$

The total cross-sectional area is:

$$A_{\text{cross}} = \frac{A_p}{\varepsilon} = \frac{\pi D_p \ell_{\max}^2}{4\varepsilon\left(2-D_p\right)}\left[1-\left(\frac{\ell_{\min}}{\ell_{\max}}\right)^{2-D_p}\right] \tag{26}$$

where ε is the areal porosity of the cross-section.

The height of fractal rough surface $z(x)$ is mainly distributed in the range form $-k\tau_h(\delta)$ to $k\tau_h(\delta)$. The asperity outside this range can be ignored. Therefore, the initial cross-section area of the contact surfaces A_{cross} is $2k\tau_h(\delta)L_0$.

Considering the squeezing force and the contact area, the effective porosity ε has the following boundary conditions:

- When two surfaces are in contact but do not squeeze each other ($F_N^* = 0$), the half of the cross-section of the contact region is occupied by asperity, as ε = 0.5.
- When two surfaces are in tight contact ($F_N^* \to \infty$), the pores are completely compressed. So ε is nearly 0.
- ε decreases with the rising of squeezing force at a certain observation scale.
- ε increases with the rising of observation scale under a certain squeezing force.

Based on these boundary conditions, the linear calculation formula of effective porosity is denoted as:

$$\varepsilon = \frac{\tau_h\left(\lambda_{c2}\right) - \tau_h\left(\lambda_{c1}\right)}{2\tau_h\left(\delta\right)}, \quad \left(\delta < \lambda_{c2} < \lambda_{c1}\right) \tag{27}$$

where λ_{c1} is the critical observation length of maximum pore, λ_{c2} is the critical observation scale of minimum pore.

The fractal dimension of the cross-section of a unit cell could be obtained by following Eq. (28) [10]:

$$D_p = d_E - \frac{\ln\varepsilon}{\ln\left(\ell_{\min}/\ell_{\max}\right)} \tag{28}$$

where d_E is the Euclidean dimension of the cross-section, $d_E = 2$.

According to percolation theory, the threshold for 2D quadrangle system is 0.593 [4,23–29]. Therefore, when the initial leak path emerges, the dimensionless real contact area A_r^* at the critical observation length λ_{c1} is 0.407.

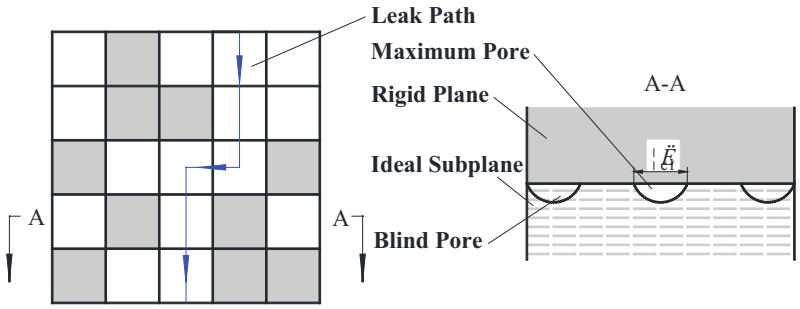

Fig. 9. Leak path at critical observation length for initial leakage.

Substitute Eq. (7) into Eq. (18) and obtain the standard normal distribution equation:

$$A_r^* = \int_{d(\lambda_{c1})}^{\infty} \frac{1}{\sqrt{2\pi}\tau_h(\lambda_{c1})} e^{-\frac{h^2(\lambda_{c1})}{2\tau_h^2(\lambda_{c1})}} dh = \int_c^{\infty} \frac{1}{\sqrt{2\pi}} e^{-\frac{h^2(\lambda_{c1})}{2}} dh = 0.407 \quad (29)$$

where c is the ratio $d(\lambda_{c1})/k\tau_h(\lambda_{c1})$, which is a constant at any observation length, as $c = 0.2353$.

The cross-section of the initial leak path is the maximum pore in the contact region. The shape of the maximum pore is composed of the profile of the asperity and the flat plane. The area of the maximum pore is:

$$A_{\text{pore,max}} = \int_{-\frac{\lambda_{c1}}{2}}^{\frac{\lambda_{c1}}{2}} h(x,\lambda_{c1})dx = \frac{2}{\pi} G^{D-1} \lambda_{c1}^{(3-D)} \quad (30)$$

The area of the maximum pore is equivalent to a circle, whose diameter is:

$$\ell_{\max} = \sqrt{4\frac{A_{\text{pore}}}{\pi}} \quad (31)$$

In general, the minimum pore diameter $\ell_{\min}$ should satisfy $\ell_{\min}/\ell_{\max} < 10^{-2}$ in porous media [30,31]. According to Eqs. (30) and (31), the critical observation scale for the minimum pore is:

$$\lambda_{c2} = \left(\frac{1}{8}\pi^2 \ell_{\min}^2 G^{1-D}\right)^{1/(3-D)} \quad (32)$$

The tortuous capillary length is [22]:

$$L(\ell) = \ell^{1-D_t} \ell_0^{D_t} \quad (33)$$

where, ℓ_0 is the sample length of a unit cell of fractal porous media, $\ell_0 = (A_{\text{unit}})^{0.5}$. D_t is the tortuosity fractal dimension of the tortuous capillary and can be calculated as follows:

$$D_t = 1 + \frac{\ln \bar{\tau}}{\ln(\ell_0/\bar{\ell})} \quad (34)$$

where $\bar{\delta}$ is the average tortuosity, $\bar{\ell}$ is the average pore/capillary size.

$$\bar{\tau} = \frac{1}{2}\left[1 + \frac{1}{2}\sqrt{1-\varepsilon} + \sqrt{1-\varepsilon}\frac{\sqrt{\left(1/\sqrt{1-\varepsilon}-1\right)^2 + \frac{1}{4}}}{1-\sqrt{1-\varepsilon}}\right] \quad (35)$$

$$\bar{\ell} = \frac{D_p \ell_{\max}}{D_p - 1}\left(k_\ell - k_\ell^{D_p}\right) \quad (36)$$

The fluid flow in a single capillary is regarded as viscous Poisseuille flow. The macroscopic flow caused by a pressure gradient can be regarded as a laminar and steady-state process and is described by Darcy's law (inertial/turbulent effects are ignored). According to Hagen–Poiseuille function [32,33], the volume leak rate through a single tortuous capillary can be expressed as:

$$q(\ell) = \frac{\pi \ell^4}{128\mu} \frac{\Delta p}{L(\ell)} \quad (37)$$

where μ is the fluid viscosity, $\Delta p/L(\ell)$ is the fluid pressure gradient of both sides of a capillary. Therefore the total flow rate Q can be acquired by integrating the single fluid flow rate $q(\ell)$, in the range of pore diameters form the minimum pore $\ell_{\min}$ to the maximum pore $\ell_{\max}$.

$$Q = -\int_{\ell_{\min}}^{\ell_{\max}} q(\ell)\, dN(\ell) \quad (38)$$

According to Darcy's law, the permeability of a porous medium could be obtained as follows:

$$\text{Pe} = \frac{\mu \ell_0 Q}{\Delta p A_{\text{unit}}} = \frac{4\varepsilon \ell_{\max}^{1+D_t}(2-D_p)}{128\ell_0^{D_t-1}(3+D_t-D_p)}\left[1-\left(\frac{\ell_{\min}}{\ell_{\max}}\right)^{2-D_p}\right]^{-1} \quad (39)$$

3. Numerical results and discussion

3.1. Surface fractal dimension with the same G

Two fractal surface profiles obtained with Eq. (3) with $G = 1.0 \times 10^{-11}$ m and $D = 1.3$ and 1.5 are plotted in Fig. 10. By increasing D from 1.3 to 1.5, more surface details can be seen in Fig. 10a.

Permeability Pe decreases with the rising of mean stress σ_0 as shown in Fig. 11. The decrease of D results in an increment of Pe in the full range of σ_0. Pe with $D = 1.5$, 1.6, and 1.7 can be clearly divided into two stages, the trend of Pe is an approximate straight line in logarithmic coordinate system. The smaller D is, the greater σ_0 is at the turning point. For $D = 1.4$, the change of Pe is more significant until σ_0 increases to 8 MPa. On the contrary, the change of Pe with $D = 1.3$ is smooth and steady when $\sigma_0 \leq 8$ MPa.

3.2. Surface fractal dimension with the same $\tau_h(\delta)$

The roughness of the surfaces generated by the same fractal roughness parameter G and different surface fractal dimensions D differs by several orders of magnitude. Therefore, in order to study the effects of the surface fractal dimension, it is supposed that the standard deviation, $\tau_h(\delta)$, is a constant, 5.0×10^{-7} m. The surface parameters are listed in Table 1. The surfaces have similar surface roughness (Ra).

Permeability (Pe) decreases with the increase of mean stress s_0, with the same $\tau_h(\delta)$ and different D, as shown in Fig. 12. Pe increases with rising of D when $\sigma_0 \geq 0.2$ MPa. When $D = 1.1$ and 1.3, the trend of Pe is an approximate straight line in logarithmic coordinate. When $D \geq 1.5$, the trend of Pe can be clearly divided into two stages by a turning point.

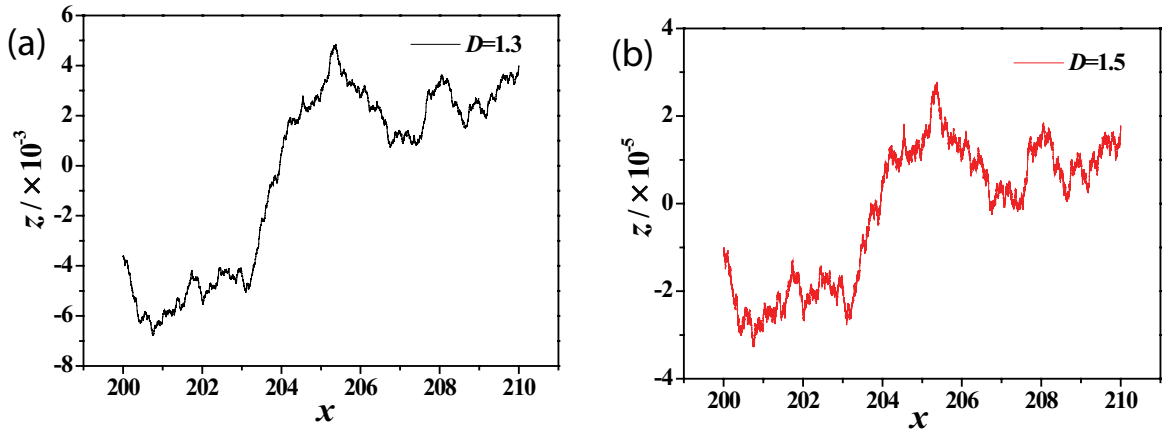

Fig. 10. Two fractal surface profiles with the same surface with: (a) D = 1.3 and (b) D = 1.5.

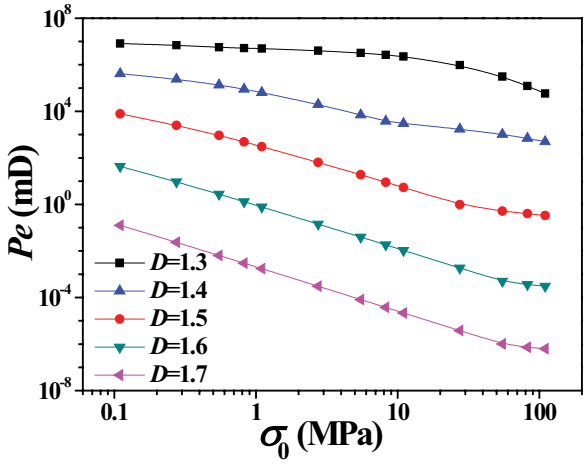

Fig. 11. Permeability vs. mean stress, with $G = 1.0 \times 10^{-11}$ m, $E^* = 110$ GPa, $\phi = 0.0010$, and $D = 1.3, 1.4, 1.5, 1.6, 1.7$.

Table 1
Surface fractal dimension and corresponding parameters

D	G (m)	Ra (m)
1.1	6.47×10^{-54}	4.42×10^{-7}
1.2	5.99×10^{-28}	4.41×10^{-7}
1.3	2.64×10^{-19}	4.38×10^{-7}
1.4	5.40×10^{-15}	4.31×10^{-7}
1.5	2.03×10^{-12}	4.23×10^{-7}
1.6	1.02×10^{-10}	4.13×10^{-7}
1.7	1.60×10^{-9}	4.06×10^{-7}
1.8	1.18×10^{-8}	4.03×10^{-7}
1.9	5.02×10^{-8}	3.96×10^{-7}

The difference of Pe with various D at the same σ_0 is very small until the turning point. In addition, the greater D is, the greater σ_0 is at the turning point. When $D = 1.9$, the trend of Pe is nonlinear in logarithmic coordinates. The surface with larger D has a higher Pe, which can be interpreted as that the complex surface topography will have a positive impact on the contact leakage characteristics. Furthermore, the surface with a greater D has a smaller surface roughness Ra but a greater Pe, with the same $\tau_h(\delta)$, as shown in Fig. 13. That means that D plays a decisive role in the influence of permeability when Ra is similar.

3.3. Effects of fractal roughness parameter G

The permeability Pe is plotted in Fig. 14, with $G = 1.0 \times 10^{-9}$, 1.0×10^{-10}, 1.0×10^{-11}, 1.0×10^{-12}, and 1.0×10^{-13} m. Increase of G can enlarge Pe at the same mean stress in the full range of σ_0. Pe decreases with the increase of σ_0, which can be clearly divided into two stages. The turning point of Pe can be seen and the corresponding σ_0 moves from 9 to 12, 30, and 60 MPa, when the value of G equals 1.0×10^{-9}, 1.0×10^{-10}, 1.0×10^{-11}, and 1.0×10^{-12} m. In the first stage, Pe and σ_0 are approximately linear in the logarithmic coordinate system. In addition, there is a better linear relationship with a lower G. In the second stage, the descent rate of Pe with increasing σ_0 significantly decreases, and the slopes of the curves are approximately equal.

4. Experiments

We have performed a leakage experiment of a clamp connector to test the model presented above. The hydraulic torque wrench provides the normal preloading force for contact seal of a clamp connector. The seal chamber is filled with water, and the pump, as shown in Fig. 15, provides its fluid pressure. Since the leakage of the liquid through the seal region is very small and hard to be measured. Therefore, considering the compressibility of the fluid, the leak rate Q can be obtained from the change of fluid volume, which can be obtained indirectly by pressure change, in the isothermal process. The pressure gauge with the precision 0.4 MPa displayed data of pressure change, which is recorded every 0.5 h when the pressure drop is stable, and a single experiment may take 5–11 h. The leak rate Q can be written as:

$$Q = \frac{\Delta V}{\Delta t} = -\kappa V(t_0)\frac{\left[p(t_1) - p(t_0)\right]}{t_1 - t_1} \tag{40}$$

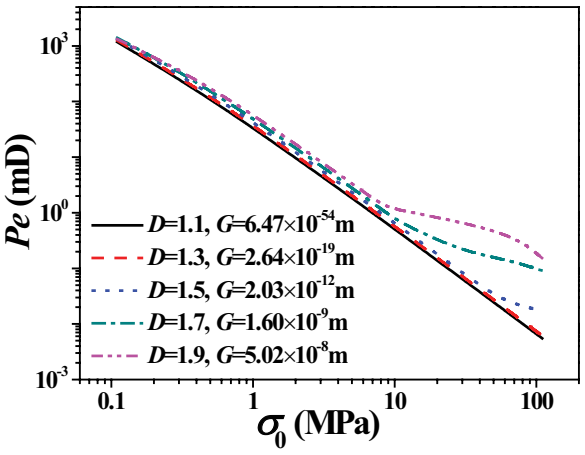

Fig. 12. Permeability vs. mean stress, with $\tau_h(\delta) = 5.0 \times 10^{-7}$ m, $E^* = 110$ GPa, $\phi = 0.0010$, $v = 0.30$, and $D = 1.1, 1.3, 1.5, 1.7, 1.9$.

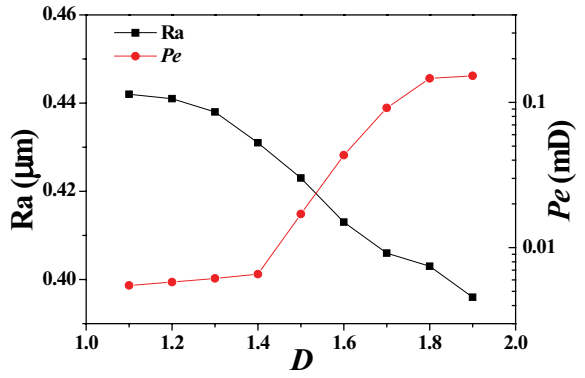

Fig. 13. Pe and Ra vs. mean stress, with $\tau_h(\delta) = 5.0 \times 10^{-7}$ m, $E^* = 110$ GPa, $\phi = 0.0010$, $\sigma_0 = 110$ MPa, and $D = 1.1, 1.3, 1.5, 1.7, 1.9$.

where ΔV is the change in water volume. $V(t_0)$ is the initial water volume in the seal chamber. p is the fluid pressure. Δt is the change of time, $\Delta t = t_1 - t_0$. κ is compressibility of water, $\kappa = 4.5 \times 10^{-10}$ m^2/N.

In order to simplify the effect of fluid pressure on flow rate, flow resistance is introduced as the ratio of fluid pressure to leakage rate, which can be written as:

$$R_f = \frac{p(t_0)}{Q} = \frac{p(t_0)\Delta t}{\Delta V} = -\frac{\Delta t}{\kappa V(t_0)}\left[\frac{p(t_1)}{p(t_0)} - 1\right]^{-1} \tag{41}$$

Considering the reaction of fluid pressure to preloading force, the contact force of the seal region is:

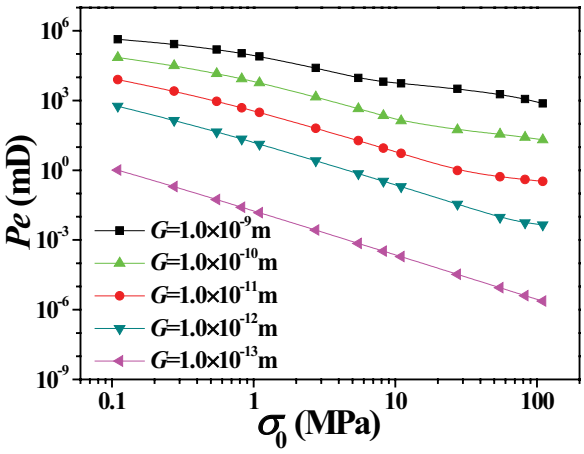

Fig. 14. Permeability vs. mean stress, with $D = 1.5$, $E^* = 110$ GPa, $\phi = 0.0010$, $v = 0.30$, and $G = 1.0 \times 10^{-9}$, 1.0×10^{-10}, 1.0×10^{-11}, 1.0×10^{-12}, 1.0×10^{-13} m.

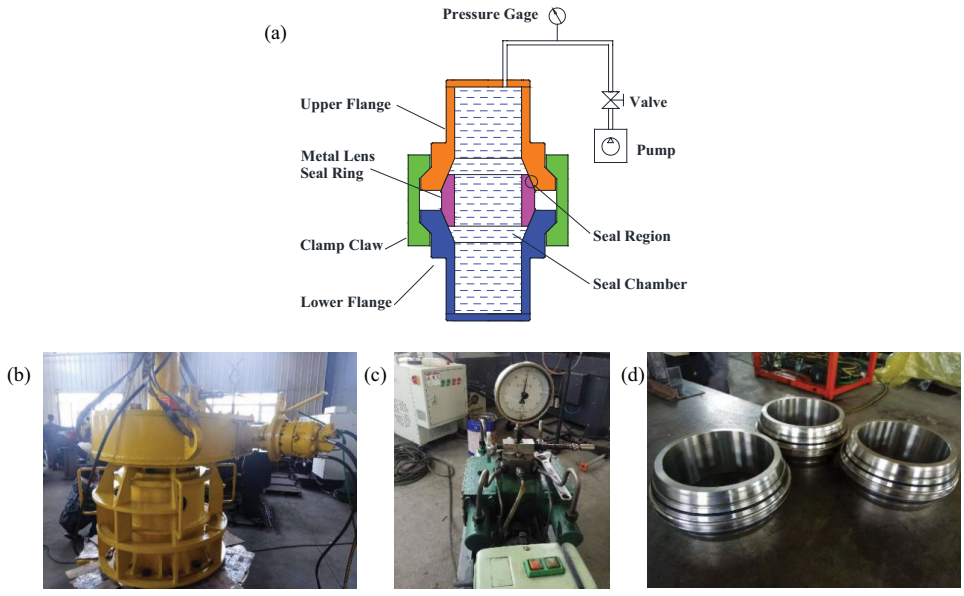

Fig. 15. Clamp connector leakage experiment. (a) Schematic diagram of experimental principle, (b) clamp connector and hydraulic torque wrench, (c) pump and pressure gauge, and (d) metal lens seal ring.

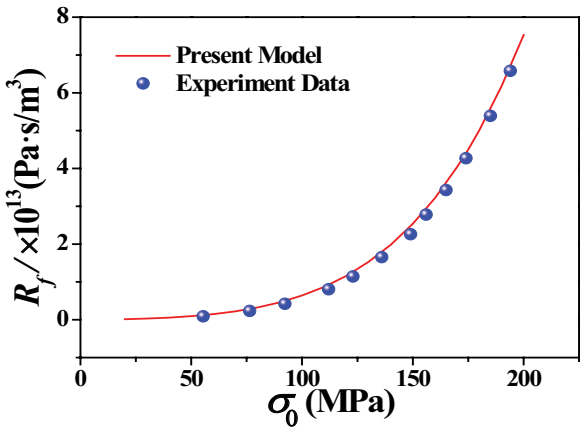

Fig. 16. Comparison of fluid resistance between the model prediction and experimental data.

$$F_L = F_0 - pS_{\text{in}} \tag{42}$$

where F_0 is the normal preloading force on seal region, S_{in} is the efficient area of the fluid acting on seal region.

The flow resistance of present model can be obtained by Eq. (39):

$$R_f = \frac{\Delta p}{Q} = \frac{\mu \ell_0}{\text{Pe} A_{\text{cross}}} \tag{43}$$

where ℓ_0 is the width of contact region, $\ell_0 = 2r$. A_{cross} is the cross-section area of contact region, $A_{\text{cross}} = 2k\tau_h(\delta)\, L$.

The hardness of metal lens seal ring is lower than the flange. Therefore, the flange can be regarded as a rigid plane, and the seal ring as a fractal deformable surface. The parameters of the surface are $D = 1.304$, $G = 1.308 \times 10^{-13}$ m, $L_0 = 1$ mm, Ra = 0.62 μm, $\tau_h(\delta) = 0.93 \times 10^{-6}$ m, $\sigma_Y = 175$ MPa, $E^* = 112$ GPa, $v = 0.3$. The initial water volume in the seal chamber $V(t_0)$ is 2.92×10^{-2} m^3.

Fig. 16 indicates that the predictions of the fluid resistance R_f of the present model are consistent with the results of clamp connector leakage experiment in trend. However, R_f predicted by present model is higher than most experiment results. The reason may be that the leakage of valve is inevitable. The difference of R_f between the present model and experiment data is small, when σ_0 is close to the yield limit σ_Y. Therefore, the present model for fluid resistance can predict the leakage mechanisms of the clamp connector within the yield limit of the deformable surface.

5. Conclusion

An OLD mechanic model and a new fractal porous media model were proposed to calculate the permeability of the contact seal consist of a rigid plane and a fractal deformable surface. The fractal surface parameters fractal dimension D, fractal roughness parameter G, and standard deviation $\tau_h(\delta)$ had significant effects on the permeability of the contact seal. The fluid resistance was applied to analyze the leakage mechanism of the clamp connector, which is a typical contact seal of the surfaces with macroscopic non-flat geometry. The leakage experiment of a clamp connector was performed, and the results showed good agreement with the prediction of the present model in trend, within the yield limit of the deformable surface.

Acknowledgment

This research was funded by [National Natural Science Foundation of China (NSFC)] grant number [5167051260], [the State Key Laboratory of Ocean Engineering (Shanghai Jiao Tong University)] grant number [1804], and [the Fundamental Research Funds for the Central Universities] grant number [HEUCFG201828].

References

[1] Z. Ji, J. Sun, C. Ma, Q. Yu, J. Lu, Key scientific problems for studying leakage mechanism of contact mechanical seal interface, CIESC J., 68 (2017) 2969–2978.
[2] X. Feng, B. Gu, Experimental research on leakage model of metallic gasket seals, Lubr. Eng., 33 (2008) 53–55.
[3] X. Feng, Study on Sealing Model and Application of Metal Gasket, PhD Thesis, Nanjing Tech University, Nanjing, 2006.
[4] J. Shi, Research on Modeling and Mechanism of Static Sealing Based on Percolation Theory, PhD Thesis, Beijing Institute of Technology, Beijing, 2015.
[5] B.N.J. Persson, Contact mechanics for randomly rough surfaces, Surf. Sci. Rep., 61 (2006) 201–227.
[6] B.N.J. Persson, C. Yang, Theory of the leak-rate of seals, J. Phys. Condens. Matter, 20 (2008).
[7] B. Lorenz, B.N.J. Persson, Leak rate of seals: comparison of theory with experiment, Europhys. Lett., 86 (2009).
[8] J.H. Tripp, Surface roughness effects in hydrodynamic lubrication: the flow factor method, J. Lubr. Technol., 105 (1983) 458–465.
[9] B.M. Yu, Comments on "a fractal geometry model for evaluating permeabilities of porous preforms used in liquid composite molding", Int. J. Heat Mass Transfer, 44 (2001) 2787–2789.
[10] B. Yu, J. Li, Some fractal characters of porous media. Fractals, 9 (2001) 365–372.
[11] X. Huang, B. Yao, G. Xu, X. Lv, Leakage of metal gaskets based on fractal porous media transport, J. Huazhong Univ. Sci. Technol. (Natural Science Edition), 44 (2016) 1–5.
[12] M. Liu, L. Wang, H. Liu, X. Ji, J. Liu, A fractal model for fluid leak rates through contact rough surfaces under a changing fluid pressure, J. Coastal Res., 83 (2018) 343–349.
[13] K.L. Johnson, Contact mechanics, J. Tribol., 108 (1985) 464.
[14] K. Lo, D.N. Mah, G. Wang, M.K.H. Leung, A.Y. Lo, P. Hills, Barriers to adopting solar photovoltaic systems in Hong Kong, Energy Environ., 29 (2018) 649–663.
[15] A.H. Kori, M.A. Jakhrani, S.A. Mahesar, G.Q. Shar, M.S. Jagirani, A.R. Shar, O.M. Sahito, Risk assessment of arsenic in ground water of Larkana City, Geol. Ecol. Landscapes, 2 (2018) 8–14.
[16] F. Yun, L. Wang, S. Yao, J. Liu, T. Liu, R. Wang, Analytical and experimental study on sealing contact characteristics of subsea collet connectors, Adv. Mech. Eng., 9 (2017).
[17] B. Fei, H. Wang, Z. Jiang, Study on fractal characteristics of machined surfaces, J. Xi'an Jiaotong Univ., 32 (1998) 85–88.
[18] Y. Zhao, D.M. Maietta, L. Chang, An asperity microcontact model incorporating the transition from elastic deformation to fully plastic flow, J. Tribol., 122 (2000) 86–93.
[19] R.L. Jackson, I. Green, A finite element study of elasto-plastic hemispherical contact against a rigid flat, J. Tribol., 127 (2005) 343–354.
[20] W.R. Chang, I. Etsion, D.B. Bogy, An elastic-plastic model for the contact of rough surfaces, J. Tribol., 109 (1987) 257–263.
[21] B. Yu, L.J. Lee, H. Cao, A fractal in-plane permeability model for fabrics, Polym. Compos., 23 (2002) 201–221.

[22] B. Yu, P. Cheng, A fractal permeability model for bi-dispersed porous media, Int. J. Heat Mass Transfer, 45 (2002) 2983–2993.
[23] D. Stauffer, A. Aharony, Introduction to Percolation Theory: Revised Second Edition, General & Introductory Physics, 1994.
[24] M.M. Parvez, M.M. Billah, M.M. Iqbal, M.M. Rahman, M.K.A. Bhuiyan, S.S. Romkey, M.A.O. Dawood, M.S. Islam, Fish diversity and water characteristics in the Reju Khal River Estuary, Bangladesh, Water Conserv. Manage., 2 (2018) 11–19.
[25] N.F.A. Rozuki, M.H. Tajuddin, N. Yusof, Effect of different solvent on asymmetric polysulfone (Psf) membranes for Co_2/Ch_4 separation, Environ. Ecosyst. Sci., 2 (2018) 11–14.
[26] J.O. Imoniana, R.R. Soares, L.C. Domingos, A review of sustainability accounting for emission reduction credit and compliance with emission rules in Brazil: a discourse analysis, J. Cleaner Prod., 172 (2018) 2045–2057.
[27] Z. Tumsavas, Application of visible and near infrared reflectance spectroscopy to predict total nitrogen in soil, J. Environ. Biol., 38 (2017) 1101–1106.
[28] S. Kanhaiya, S. Singh, C.K. Singh, V.K. Srivastava, A. Patra, Geomorphic evolution of the Dongar River Basin, Son Valley, Central India, Geol. Ecol. Landscapes, 3 (2019) 269–281, doi: 10.1080/24749508.2018.1558019.
[29] C. Bao, X. Meng, J. Li, X. Peng, Study on leakage rate of liquid lubricated mechanical seal based on percolation theory, Fluidmachinery, (2014) 24–28.
[30] A.J. Ali, N.J. Akbar, M.S.A. Kumar, S. Vijayakumar, B.A. John, Effect of cadmium chloride on the haematological profiles of the freshwater ornamental fish, *Cyprinus carpio* Koi (Linnaeus, 1758), J. Clean WAS, 2 (2018) 10–15.
[31] B. Yu, Fractal Porous Media Transport Physics, Science Press, Beijing, 2014.
[32] Q. Zheng, J. Xu, B. Yang, B. Yu, A fractal model for gaseous leak rates through contact surfaces under non-isothermal condition, Appl. Therm. Eng., 52 (2013) 54–61.
[33] C.C. Okpoli, Delineation of high-resolution aeromagnetic survey of lower benue trough for lineaments and mineralization: case study of Abakikili Sheet 303, Malaysian J. Geosci., 3 (2019) 51–60.